SCIENCE CHINA
Information Sciences

• LETTER •

August 2026, Vol. 69, Iss. 8, 189401:1–189401:2
https://doi.org/10.1007/s11432-025-4709-4

# Frequency scaling and elastic transition in HF–VHF $WS_2$ NEMS resonators

Jiankai ZHU[1,2†], Chenfei LV[1†], Ziluo SU[1†], Bo XU[1], Fei XIAO[3*], Hao JIA[2*] & Zenghui WANG[1*]

[1]*Institute of Fundamental and Frontier Sciences, University of Electronic Science and Technology of China, Chengdu 610054, China*
[2]*State Key Laboratory of Transducer Technology, Shanghai Institute of Microsystem and Information Technology, Chinese Academy of Sciences, Shanghai 200240, China*
[3]*Hangzhou Institute of Technology, Xidian University, Hangzhou 311200, China*

Received 19 August 2025/Revised 22 October 2025/Accepted 5 December 2025/Published online 15 July 2026

**Citation** Zhu J K, Lv C F, Su Z L, et al. Frequency scaling and elastic transition in HF–VHF $WS_2$ NEMS resonators. Sci China Inf Sci, 2026, 69(8): 189401, https://doi.org/10.1007/s11432-025-4709-4

Two-dimensional transition-metal dichalcogenides (2D TMDCs) offer promising opportunities for novel nanodevices. Among them, tungsten disulfide ($WS_2$, crystal structure in Figure 1(a)) is particularly interesting, due to the highest predicted carrier mobility, excellent FET performance, and capability of forming memristive transistors when integrated with ferroelectric materials [1]. Further development of $WS_2$ nanodevices with mechanical degrees of freedom is expected to leverage the high sensitivity and responsivity from structural deformation [2]. However, $WS_2$-based nanoelectromechanical system (NEMS) devices remain limited, with frequency scaling and tunability largely unexplored. Here, we demonstrate $WS_2$ NEMS resonators operating in high- and very-high-frequency (HF–VHF) bands, and extract the device pretension and the Young's modulus of 2D $WS_2$ crystal, as well as delineate and validate the devices's frequency tunability via electrostatic tuning. Our results elucidate design rules for functional NEMS devices based on $WS_2$ 2D crystals, and reveal the high frequency tunability (∼36% from 0 to 10 V) exhibited by the device in the transition regime.

*Devices and experiments.* A total of 30 circular drumhead $WS_2$ resonators (Figure 1(b)) with varying diameters and thicknesses are fabricated using mechanical exfoliation and dry transfer (Figure S1(a)). Their thicknesses range from monolayer to over 200 layers in two structures (Figures 1(b) and (c)), as determined by atomic force microscopy for thicker samples (Figure S1(d)) and Raman spectroscopy for thinner ones (<6 layers; Figure 1(d)) [3].

We examine the resonant behavior of NEMS $WS_2$ devices using a custom-built NEMS measurement system based on laser interferometry (Figure S2). Device motion is excited either electrostatically or optothermally using a 405 nm laser, and is detected interferometrically using a 633 nm laser. Through fitting we extract the fundamental mode resonance frequency (along with quality factor) for each device, which spans from 2.28 to 40.90 MHz (Figure S3 and Table S1), covering both HF and VHF bands.

*Theoretical analysis.* To quantitatively extract the elastic properties of 2D $WS_2$ crystals and to understand the frequency scaling law in these devices, we conduct a theoretical analysis. For a circular drumhead resonator of radius $r$ and thickness $t$, the fundamental mode frequency can be expressed as

$$f_0 = \left(\frac{(kr)}{2\pi}\right)\sqrt{\frac{D}{\sigma r^4}\left[(kr)^2 + \frac{\gamma r^2}{D}\right]} = \sqrt{f_{\text{plate}}^2 + f_{\text{membrane}}^2}, \quad (1)$$

where $\sigma = \rho t$ is the drumhead's areal mass density ($\rho$: volumetric mass density); $\gamma$ (N/m) is the 2D tension, and $D = E_{\text{Y}}t^3/[12(1-\nu^2)]$ is the flexural rigidity with $E_{\text{Y}}$ the Young's modulus and $\nu$ the Poisson's ratio. $(kr)$ is a mode-dependent parameter determined numerically. The fundamental frequency $f_0$ comprises two terms, $f_{\text{plate}}$ and $f_{\text{membrane}}$, corresponding to the plate- and membrane-dominated limits, respectively.

*Results and discussion.* We examine the plate-dominated limit ($\gamma r^2/D \to 0$), in which the fundamental frequencies vary linearly with $t/r^2$, consistent with theoretical expectations (Eq. (S3)). From this relationship, we extract the Young's modulus from ten devices (thicker than 10 nm, marked with * in Table S1) and obtain an average value of 141.7 GPa (Figure 1(f)), with a standard error $SE = s/\sqrt{N} = 19.5$ GPa ($s$: standard deviation). We find that this Young's modulus is lower than that of 1–3 L $WS_2$, consistent with previous observations showing a pronounced decrease with increasing thickness [4]. We further compare the data with the full model, which gives pretensions of $\gamma = 0.02$–$0.5$ N/m, consistent with values reported for exfoliated and dry-transferred 2D resonators [5].

Building on the extracted parameters, we analyze the size dependence of the resonance frequency by combining theory and experiment (Figure 1(e)). This reveals the intrinsic evolution from the membrane-dominated regime to the transition regime and ultimately to the plate-dominated regime with increasing thickness. The distribution of our 30 devices across these three regimes is shown in Figure 1(g). These results (Figures 1(e) and (g)) provide clear guidelines for the device design of future NEMS devices based on 2D $WS_2$.

We examine electrostatic tuning using one resonator from the transition regime (Device 1) and one from the plate regime (Device 2) (Figure 1(h)). Device 1 exhibits a clear electrostatic frequency

* Corresponding author (email: xiaofei@xidian.edu.cn, hao.jia@mail.sim.ac.cn, zenghui.wang@uestc.edu.cn)
† These authors contributed equally to this work.

 

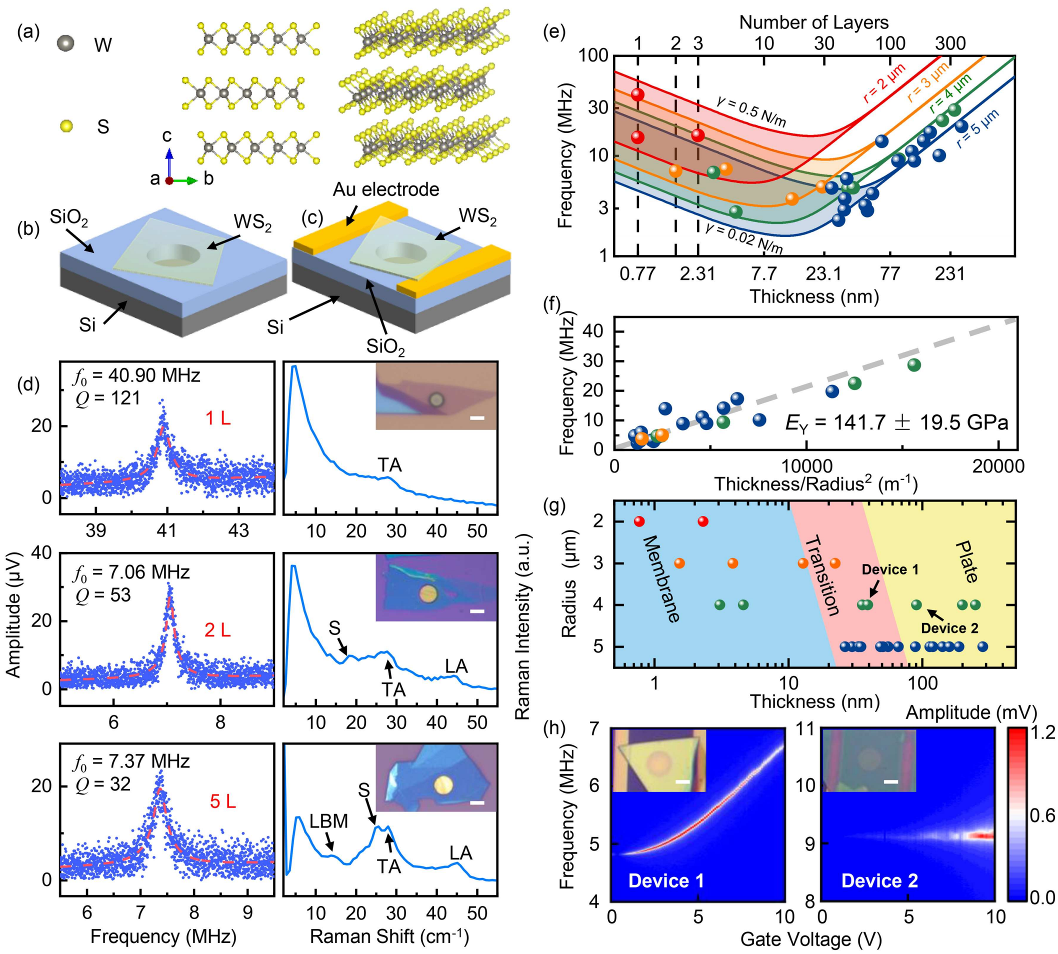


**Figure 1** (Color online) Structural and mechanical characterization of few-layer $WS_2$ resonators. (a) Crystal lattice of $WS_2$. (b) and (c) Device structures of circular drumhead $WS_2$ resonators without and with electrodes. The former is actuated solely by optothermal driving, while the latter supports both optothermal and capacitive electrostatic actuation (details in Figure S2). (d) Resonant responses (left) and low-frequency Raman spectra (right) for monolayer (1 L), bilayer (2 L), and multilayer (5 L) devices. Insets: optical images of the corresponding devices (scale bar: 5 μm). Blue and red denote raw and fitted data, respectively. (e) Frequency scaling law of $WS_2$ resonators. Solid lines indicate the calculated fundamental mode frequency under pretensions of 0.02 N/m (lower bound) and 0.5 N/m (upper bound). Device radii are color coded: red (2 μm), orange (3 μm), green (4 μm), and blue (5 μm). (f) Measured resonance frequencies as a function of $t/r^2$. The fitting curve (gray dashed line) gives a Young's modulus of $141.7 \pm 19.5$ GPa for 2D $WS_2$ crystal. (g) Calculated elastic regimes of the devices (assuming $\gamma = 0.3$ N/m). Plate regime (yellow): $f_{\rm plate} \geqslant 0.97\, f_0$; transition regime (pink): both $f_{\rm plate}$ and $f_{\rm membrane} \leqslant 0.97\, f_0$; membrane regime (blue): $f_{\rm membrane} \geqslant 0.97\, f_0$. (h) Gate tuning responses of Device 1 (from transition regime) and Device 2 (from plate regime). Optical images (scale bar: 10 μm) of the devices are shown as insets, and detailed device information is provided in Supporting information.

tuning (∼36% from 0 to 10 V), while Device 2 shows only an increased amplitude without a significant frequency shift. Using Eq. (1) and assuming the in-plane stress increases from 0.02 to 0.6 N/m, we calculate tuning ranges of 36.4% and 1.0% for Devices 1 and 2, respectively. While other effects such as capacitive softening also affect tuning, our observation clearly shows the contrast between different elastic regimes and reveals the critical role of the membrane component $f_{\rm membrane}$ in frequency tuning.

*Conclusion*. We fabricate and investigate 2D $WS_2$-based NEMS resonators operating in the HF to VHF bands, extract their mechanical parameters, and reveal their frequency scaling law, elastic transitions, and frequency tunability.

**Acknowledgements** This work was supported by National Key R&D Program of China (Grant No. 2022YFB3203600), National Natural Science Foundation of China (Grant Nos. 62401104, 62404174, 62404029, 62104241), Opening Foundation of State Key Laboratory of Transducer Technology (Grant No. SKT2309), Sichuan Science and Technology Program (Grant Nos. 2024NSFSC1430, 2024NSFSC1408), and China Postdoctoral Science Foundation (Grant Nos. GZB20240109, GZC20250382).

**Supporting information** Figures S1–S7, Table S1. The supporting information is available online at info.scichina.com and link.springer.com. The supporting materials are published as submitted, without typesetting or editing. The responsibility for scientific accuracy and content remains entirely with the authors.

## References


1 Hoang L, Jaikissoon M, Köroğlu Ç, et al. Understanding the impact of contact-induced strain on the electrical performance of monolayer $WS_2$ transistors. Nano Lett, 2024, 24: 12768–12774
2 Nathamgari S S P, Dong S, Medina L, et al. Nonlinear mode coupling and one-to-one internal resonances in a monolayer $WS_2$ nanoresonator. Nano Lett, 2019, 19: 4052–4059
3 Tan Q H, Sun Y J, Liu X L, et al. Observation of forbidden phonons, Fano resonance and dark excitons by resonance Raman scattering in few-layer $WS_2$. 2D Mater, 2017, 4: 031007
4 Falin A, Holwill M, Lv H, et al. Mechanical properties of atomically thin tungsten dichalcogenides: $WS_2$, $WSe_2$, and $WTe_2$. ACS Nano, 2021, 15: 2600–2610
5 Tang J, Su Z L, Cai S, et al. HF-VHF NEMS resonators enabled by 2D semiconductor $ReSe_2$. Sci China Inf Sci, 2024, 67: 209401